Science and Technology Indonesia
e-ISSN:2580-4391 *p*-ISSN:2580-4405
Vol. 11, No. 1, January 2026

Research Paper

Determination of Paraquat Using Microfluidic Paper-Based Analytical Device (μPAD) Immobilized with *p*-Hydroxybenzoic Acid Capped Silver Nanoparticles

Gusrizal Gusrizal[1], Firman Shantya Budi[1*], Dewi Puspita[1]

[1]*Department of Chemistry, Faculty of Mathematics and Natural Sciences, Universitas Tanjungpura, Pontianak, 78124, Indonesia*
***Corresponding author**: firmanshantyabudi@fmipa.untan.ac.id

Abstract
This study developed a microfluidic paper-based analytical device (μPAD) immobilized with *p*-hydroxybenzoic acid capped silver nanoparticles (AgNPs-PHB) for the colorimetric detection of paraquat (PQ) in water samples. The synthesized AgNPs-PHB exhibited favorable properties, including a nanoscale size (68.5 nm by DLS, 20 nm by TEM), high stability (zeta potential of -53 mV), and a spherical morphology, as confirmed by UV-Vis spectroscopy, PSA, and TEM analysis. The μPAD platform utilized a wax-printed hydrophobic barrier to direct sample flow, enabling a simple and cost-effective detection method. Upon interaction with PQ, AgNPs-PHB underwent aggregation, resulting in a visible color change from yellow to gray, which was quantified using ImageJ software for RGB analysis. The method demonstrated excellent linearity (R^2 = 0.9917 for red intensity) across a concentration range of 0.001 - 0.01 M, with a limit of detection (LOD) of 0.00060 M and a limit of quantification (LOQ) of 0.0020 M. Precision tests revealed high repeatability and reproducibility, with intraday and interday %RSD values below 2%. Recovery studies in tap water, drainage water, and well water samples spiked with PQ yielded accurate results (99.7–102.5%), validating the method's reliability. Compared to conventional techniques, this μPAD-based approach offers a portable, environmentally friendly, and sensitive alternative for monitoring PQ contamination in environmental water samples, making it suitable for field applications.

Keywords
Paraquat, Silver Nanoparticles, μPAD, Colorimetric Detection, Water Analysis

Received: 23 August 2025, Accepted: 20 December 2025
https://doi.org/10.26554/sti.2026.11.1.323-334

1. INTRODUCTION

Paraquat (1,1'-dimethyl-4,4'-bipyridinium dichloride, PQ) is a bis-quaternary ammonium compound that has been widely used as a domestic and commercial herbicide (Rahman et al., 2024). PQ belongs to the class of quaternary ammonium salts that bind chloride anions (Cl^-), with its nomenclature derived from the para position of its quaternary nitrogen atoms (Figure 1). In recent years, paraquat has become a major environmental and public health concern due to its extreme toxicity and persistence. Even small doses of PQ (15–20 mL of a 20% solution) can be fatal, as it causes systemic damage to vital organs such as the lungs, liver, and kidneys through the excessive generation of reactive oxygen species (ROS), leading to oxidative stress and lipid peroxidation (Chandra et al., 2021). Despite regulatory restrictions, paraquat continues to be used in several Asian and Latin American countries because of its effectiveness against herbicide-resistant weeds and its low cost (Stuart et al., 2023). The compound is highly persistent in the environment, with a soil half-life exceeding seven years, and it exhibits strong adsorption to soil particles while remaining capable of leaching into aquatic ecosystems, thereby posing risks to non-target organisms, including fish, birds, and invertebrates (Franco et al., 2022).

Recent studies have reported paraquat residues in various agricultural commodities, particularly soy-based animal feed imported from major producing countries such as Brazil and the United States (Heydebreck, 2021). This raises serious concerns over indirect exposure through the food chain. Although more than 60 countries have banned or restricted its use, paraquat remains widely applied in some regions due to its efficacy and low cost (Stuart et al., 2023). Moreover, recent advances in adsorption-based technologies using biochar, bentonite, and carbon nanomaterials have shown promising potential for removing paraquat from contaminated water (Franco et al., 2022). Consequently, numerous countries, including Indonesia, have imposed restrictions on paraquat use to protect environmental and human health, underscoring the importance of advancing effective remediation technologies and adopting safer agricultural practices to reduce its worldwide impact.

Several methods have been employed to determine PQ levels quantitatively, including chromatography and spectrophotometry. The determination of PQ using UV-VIS spectrophotometry (Gusrizal et al., 2020; Khatoon et al., 2013; Lima et al., 2018), chromatography, including HPLC (Yar et al., 2022), UHPLC-MS/MS (Pan et al., 2022; Pizzutti et al., 2016; Zhao et al., 2023), and HPLC-ESI/MS (Takino et al., 2000). Common limitations of UV-VIS spectrophotometry and modern chromatography methods include the high cost of equipment, the need for skilled operators, and the requirement for a large amount of solvents. Therefore, it is necessary to explore alternative methods that are more cost-effective and easier to perform.

Currently, the microfluidic paper analytical devices (μPAD) method is a simple, inexpensive, easy-to-use analysis method that does not require modern instruments and can analyze a substance on a microliter scale (Sununta et al., 2018). μPAD is a paper-based analysis device consisting of a hydrophilic channel (detection zone) and a hydrophobic barrier. μPAD uses filter paper or chromatography paper, where the hydrophobic pattern is designed using computer software and printed using wax printing, while the hydrophilic part serves as the detection zone for the substance and the immobilized reagent zone (Anushka et al., 2022). The use of wax printing in creating the hydrophobic pattern serves as a barrier, preventing the sample solution and reagents from penetrating and directing the flow of the solution. As a result, the solution flows through the hydrophilic zone (detection zone) via capillary action.

The use of the μPAD method for the quantitative determination of pesticides has been reported, where the determination of carbamate pesticides using μPAD, including carbaryl, carbofuran, and furathiocarb, yielded detection limits of 0.4, 0.24, and 0.46 mg/L, respectively (Beshana et al., 2022). Additionally, μPAD has been used for the detection of atrazine pesticides in water using silver nanoparticles (AgNPs) and gold nanoparticles (AuNPs). The detection limits obtained from this study were 3.5 μM for AgNPs and 10.9 μM for AuNPs (Moulahoum, 2023)). Based on research conducted, the researchers will analyze the pesticide paraquat using silver nanoparticles capped with *p*-hydroxybenzoic acid (PHB) via μPAD. Silver nanoparticles (AgNPs) capped with *p*-hydroxybenzoic acid (PHB) were synthesized using a bottom-up technique to form AgNPs-PHB (Gusrizal et al., 2020). PHB was selected as both a reducing and capping agent due to its phenolic hydroxyl group, which effectively reduces Ag^+ ions while simultaneously stabilizing the formed nanoparticles through strong coordination with the silver surface. Previous studies have demonstrated that AgNPs-PHB exhibit excellent stability, uniform particle size distribution, and high resistance to aggregation compared to nanoparticles synthesized with conventional capping agents such as citrate or polyvinylpyrrolidone (Gusrizal et al., 2016).

While Gusrizal et al. (2020) successfully applied AgNPs–PHB for para-quat determination in solution using conventional spectrophotometric measurements, the present study introduces a more portable and environmentally friendly analytical approach. The novelty of this work lies in the development of a paper-based colorimetric sensor that integrates AgNPs–PHB into a μPAD platform, allowing quantitative detection of paraquat through color intensity analysis captured by a smartphone camera. This innovation enables rapid, low-cost, and on-site monitoring of paraquat without the need for sophisticated laboratory instruments, representing an advancement toward accessible and sustainable analytical methods.

The μPAD method to be used in this study begins with the reaction of PQ and AgNPs-PHB. The reaction results in the formation of an aggregation. A number of microlitres of AgNPs-PHB solution are immobilized on the detection zone (hydrophilic) that has been patterned and then reacted with PQ at various concentrations. This reaction changes the color of AgNPs from yellow to grey, which is clearly visible on the μPAD paper medium. Digital images of the μPAD are captured using a digital camera or smartphone camera. The intensity of the color produced by the colorimetric reaction can be correlated with the concentration of paraquat and measured using ImageJ software to obtain RGB (Red, Green, Blue) data. This study aims to analyze PQ concentrations in water samples using colorimetry with the μPAD device as a simple, fast, and environmentally friendly detection platform. Additionally, this method is designed to assess water quality by examining the presence of PQ residues as an indicator of pesticide contamination.

2. EXPERIMENTAL SECTION

2.1 Materials

All chemicals used in this study were of high purity and classified as analytical grade. All solutions were prepared using deionized water. *p*-Hydroxybenzoic acid, silver nitrate ($AgNO_3$), and sodium hydroxide (NaOH) were purchased from Merck (Germany), while paraquat was obtained from Sigma-Aldrich (USA). The paper substrate used was Whatman 1Chr Chromatography Paper (Whatman International Ltd., Maidstone, England). Printer ink type NPG-67 was used to print the microfluidic patterns on the paper. Water samples were collected from the local environment and analyzed directly using the developed method.

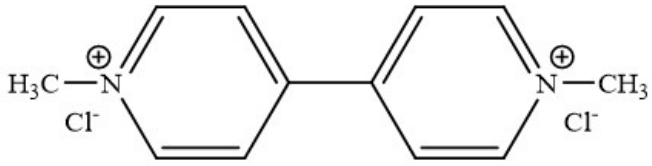

Figure 1. Structure of Paraquat Compound

2.2 Instruments

The tool used in this study included an analytical balance (Ohaus Pioneer), oven (Mammert), micropipette, pH meter, hotplate, magnetic stirrer, photobox, smartphone (OPPO Reno

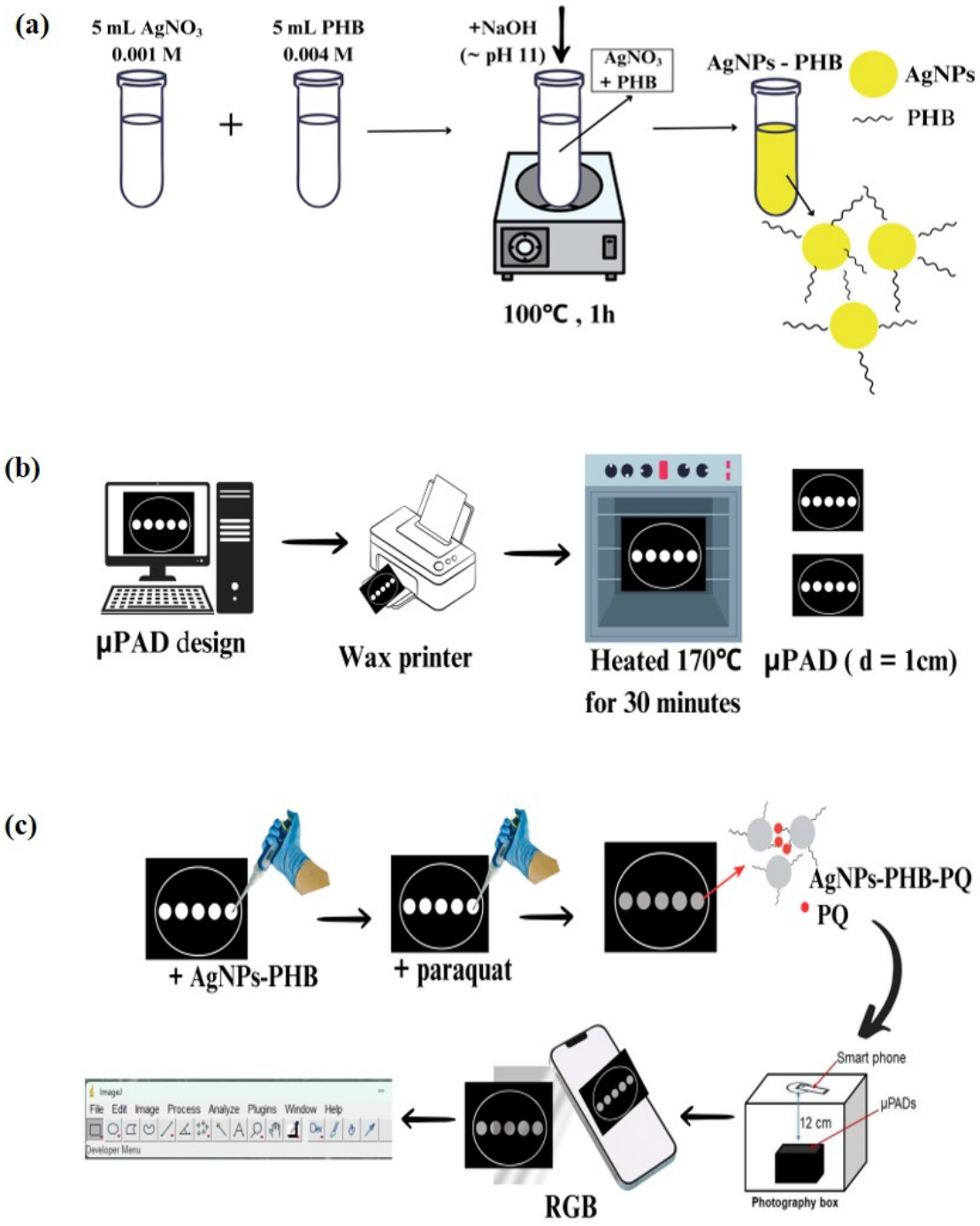

Figure 2. Synthesis of AgNPs-PHB, b) μPAD Design, c) Colorimetric Detection of Paraquat

8 Pro, 50 MP camera), wax printer (Canon ImageRUNNER C3020), ImageJ software, Microsoft PowerPoint 2019, Particle Size Analyzer (PSA, Horiba Scientific SZ-100) to determine the particle size of AgNPs-PHB, zeta potential (Horiba Scientific SZ-100) to determine the dispersion stability of AgNPs-PHB, UV-Vis Spectrophotometer-Vis (Thermo Scientific Aquamate 8100) to obtain surface plasmon resonance spectra data of AgNPs-PHB, Attenuated Total Reflectance – Infrared (ATR-IR, Bruker Alpha II, Zn/Se) to determine functional group AgNPs-PHB and AgNPs-PHB-PQ, Transmission Electron Microscope (TEM, JEOL JEM-1400) to determine the size and morphology of AgNPs-PHB.

2.3 Methods

2.3.1 Preparation of *p*-Hydroxybenzoic Acid Capped Silver Nanoparticles (AgNPs-PHB)

P-Hydroxybenzoic acid capped silver nanoparticles (AgNPs-PHB) were prepared using the procedure by Gusrizal et al. (2020). Silver nanoparticles were synthesized by reducing Ag^+ ions to Ag^0. First, 5 mL of 1×10^{-3} M $AgNO_3$ solution was added to 5 mL of 4.0×10^{-3} M *p*-hydroxybenzoic acid solution, which had been adjusted to pH 11 by adding 5M NaOH solution. The reaction mixture was heated in a boiling water bath (100 °C) for 1 hour, until the solution changed from colorless to a yellow color. It was then cooled and stored at room temperature. The synthesis process of AgNPs-PHB is shown in Figure 2a.

2.3.2 Characterization *p*-Hydroxybenzoic Acid Capped Silver Nanoparticles (AgNPs-PHB)

The formed AgNPs-PHB were characterized using a UV-Vis Spectrophotometer (Thermo Scientific Aquamate 8100) with a wavelength range of 300–750 nm. The formation of AgNPs-PHB was indicated by a peak wavelength of 400–450 nm. The particle size of AgNPs-PHB was measured using a Particle Size Analyzer (PSA, Horiba Scientific SZ-100). The dispersion stability of AgNPs-PHB was determined using zeta potential (Horiba Scientific SZ-100). Functional group was determined using Attenuated Total Reflectance – Infrared (ATR-IR, Bruker Alpha II, Zn/Se). The morphology of AgNPs-PHB was examined using a Transmission Electron Microscope (TEM, JEOL JEM-1400).

2.3.3 Design and Fabrication of μPAD

The μPAD pattern was designed using Microsoft PowerPoint 2019. The μPAD design consists of 40 detection zones with a diameter of 10 mm and a barrier zone. The pattern is then printed using a wax printer on Whatman 1Chr Chromatography Paper. The paper with the printed pattern is heated in an oven at 170 °C for 30 minutes (the ink can penetrate the filter paper and form a hydrophobic barrier that controls fluid flow). The μPAD design is shown in Figure 2b.

2.3.4 Colorimetric Determination of Paraquat

A total of 9.0 μL of AgNPs-PHB solution was deposited on the detection zone and allowed to dry for 5 minutes. Then, paraquat standards at concentrations of 6.0 μL (1.0×10^{-3}, 2.0×10^{-3}, 4.0×10^{-3}, 6.0×10^{-3}, 8.0×10^{-3}, 1.0×10^{-2} M) were added to the detection zone until a color change to grey occurred. The reaction is allowed to proceed for 10 minutes. For analysis, a mobile phone camera is used to capture images of the µPAD (12 cm from the object) inside the photobox (Figure 2c). The intensity of the color produced is measured using ImageJ software to obtain RGB data in the detection zone. The RGB values obtained are then converted into color absorption intensity (IR, IG, and IB), which were determined using Equations (1), (2), and (3).

$$I_R = \log \frac{R_0}{R_S} \quad (1)$$

$$I_G = \log \frac{G_0}{G_s} \quad (2)$$

$$I_B = \log \frac{B_0}{B_S} \quad (3)$$

(RGB)0 and (RGB)s are the color component intensities of the blank and sample. The color absorption intensities obtained are then plotted against the standard paraquat concentrations to form a standard curve (Firdaus et al., 2019). Water samples were analyzed using tap water, drainage water, and well water samples. The water samples were spiked with paraquat standards of known concentrations (2.0×10^{-3}, 4.0×10^{-3}, and 8.0×10^{-3} M). This treatment produced accuracy data expressed as recovery percentages, as calculated using Equation (4).

$$\%Recovery = \frac{C_1 - C_2}{C_3} \quad (4)$$

C_1 is the concentration of the analyte in the sample after the addition of the PQ standard, C_2 is the concentration of the analyte in the original sample, and C_3 is the concentration of the PQ standard added.

2.3.5 Analytical Method Validation

Linearity is obtained from the standard curve plot between standard PQ concentrations (X axis) and intensity (Y axis). Linear regression analysis is used to derive the Equation y = bx + a, where b represents the slope and a represents the y-intercept. The limit of detection (LOD) and limit of quantification (LOQ) are determined based on the formulas in Equations (5) and (6).

$$LOD = \frac{3 \times SD}{Slope} \quad (5)$$

$$LOQ = \frac{10 \times SD}{Slope} \quad (6)$$

SD is the standard deviation of the intercept results of linear regression analysis. Precision tests were conducted to determine repeatability (intraday precision) and reproducibility (interday precision) (Kumar Majumder et al., 2020). Repeatability is obtained by determining the standard intensity of PQ (1.0×10^{-3}, 6.0×10^{-3}, and 1.0×10^{-2} M) in six replicates at six different times within one day, while reproducibility was obtained by determining the standard PQ intensity (1.0×10^{-3},

Table 1. Color intensity of PQ standard (average n = 3)

PQ Standar (mole L^{-1})	Color Value			PQ Standar (mole L^{-1})	Color Intensity		
	R	G	B		R	G	B
Blank	213.2	206.1	184.9	Blank	0.0000	0.0000	0.0000
0.001	207.9	202.5	194.1	0.001	0.0109	0.0076	0.0209
0.002	206.4	202.4	191.4	0.002	0.0140	0.0078	0.0149
0.004	198.3	191.5	177.3	0.004	0.0315	0.0319	0.0183
0.006	190.7	184.7	170.5	0.006	0.0484	0.0476	0.0352
0.008	187.4	182.8	170.8	0.008	0.0558	0.0520	0.0345
0.01	179.9	176.9	167.9	0.01	0.0735	0.0661	0.0419

Table 2. %RSD Values for Repeatability (Intraday Precision)

PQ (mole L^{-1})	Color Intensity						Average	%RSD
	I (8 am)	II (10 am)	III (12 am)	IV (2 pm)	V (3 pm)	VI (4 pm)		
1.0×10^{-3}	0.0110	0.0112	0.0111	0.0113	0.0112	0.0110	0.0113	1.08%
6.0×10^{-3}	0.0484	0.0495	0.0478	0.0489	0.0476	0.0490	0.0485	1.79%
1.0×10^{-2}	0.0737	0.0749	0.0725	0.0742	0.0728	0.0745	0.0738	1.96%
							%RSD Average	1.61%

6.0×10^{-3}, and 1.0×10^{-2} M) in six replicates on six different days. The parameter obtained from the precision test was the %RSD (Relative Standard Deviation), which was calculated using Equation (7).

$$\%RSD = \frac{SD}{\mu} \times 100\% \quad (7)$$

SD is the standard deviation of the measurement results, and μ is the average of the measurement results.

3. RESULT AND DISCUSSIONS

3.1 Synthesis and Characterization of *p*-Hydroxybenzoic Acid Capped Silver Nanoparticles (AgNPs-PHB)

Silver nanoparticles (AgNPs) were chemically synthesized using a bottom-up approach through the reduction reaction of silver nitrate ($AgNO_3$) using *p*-hydroxybenzoic acid (PHB). $AgNO_3$ acted as a precursor source of Ag^+ ions, while PHB acted as a reducing agent and stabilizer (capping agent). Under basic conditions (pH 11), the addition of $AgNO_3$ solution to the PHB mixture triggers a reaction between $AgNO_3$ and NaOH, forming silver oxide (Ag_2O). The $AgNO_3$ compound undergoes hydrolysis in an aqueous medium, releasing Ag^+ ions that serve as the metal source for the growth of AgNPs (Gusrizal et al., 2020). In Figure 3, the hydroxyl groups (R-OH) of PHB are oxidized to carbonyl groups (R2-C=O), followed by the reduction of Ag^+ ions to Ag^0 (Gusrizal, 2017; Zhang et al., 2025). As the reduction of Ag^+ ions progresses, an increasing number of silver atoms aggregate to form initial clusters or nuclei. At this stage, Ag^0 undergoes particle growth, leading to the formation of AgNPs (Madaniyah et al., 2025). Concurrently, PHB molecules adsorb onto the surface of AgNPs, resulting in the formation of AgNPs–PHB, which enhances nanoparticle stability and inhibits further aggregation (Gusrizal et al., 2020). The interaction between PHB and the silver nanoparticle surface occurs through the carboxyl group, forming RCOO–Ag coordination bond (Gusrizal, 2017; Wang et al., 2003; Zhang et al., 2025). Based on the experimental results supported by computational simulation data, it could be concluded that the interaction between PHB and the silver nanoparticle surface occurs through the deprotonated carboxyl group, while the hydroxyl group does not play a significant role in the interaction (Goulet and Aroca, 2004). AgNPs–PHB remained stable for up to 40 weeks without the addition of any external stabilizing agents, demonstrating that PHB effectively functions as a capping agent capable of maintaining nanoparticle size and stability by preventing agglomeration (Gusrizal et al., 2018).

The synthesized AgNPs-PHB must be characterized using a UV-Vis spectrophotometer, Attenuated Total Reflectance – Infrared (ATR-IR), Particle Size Analyzer (PSA), Zeta Potential, and TEM. The UV-Vis spectrophotometer was used to identify the SPR (Surface Plasmon Resonance) peaks of AgNPs-PHB. When AgNPs-PHB formed, a color change occurred from colorless to yellow. The characterization of AgNPs-PHB resulted in an SPR absorption peak at a wavelength of 424 nm with an absorbance of 0.405 (Figure 4a). The appearance of a strong and symmetrical peak at 424 nm

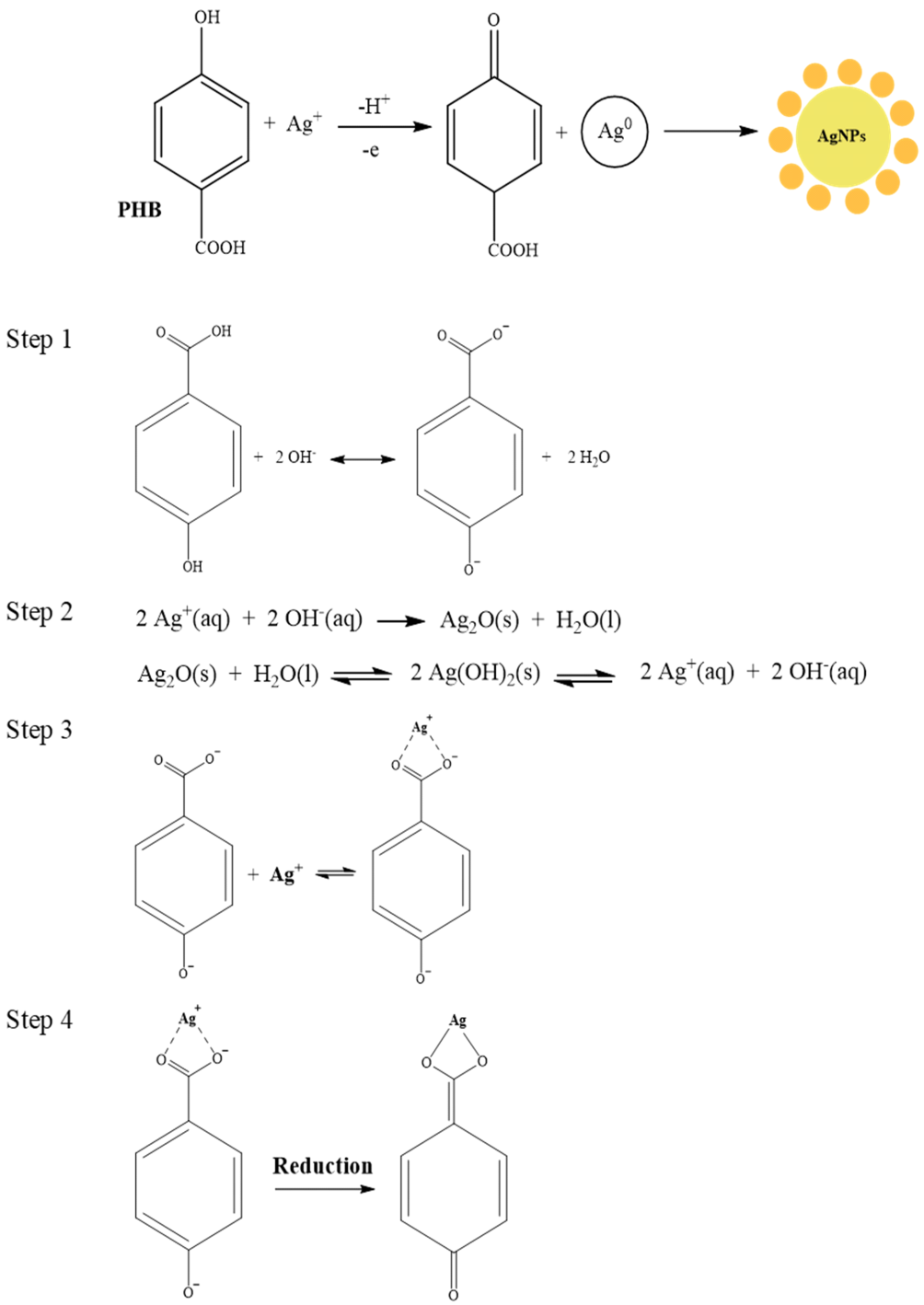

Figure 3. Formation Reaction of *p*-Hydroxybenzoic Acid Capped Silver Nanoparticles (AgNPs-PHB)

in this study indicates that the synthesized AgNPs-PHB are at the nanometre scale (<100 nm) and do not undergo significant aggregation. At the nanoscale, free electrons on the particle surface can collectively oscillate when exposed to light, resulting in characteristic absorption peaks in the UV–Vis region (Paramelle et al., 2014).

TEM images (Figure 4b) show that AgNPs–PHB have a spherical morphology with an average core size of approximately 20 nm. This size is smaller than that obtained from DLS (68.5 nm). This difference occurs because DLS measures the particle diameter along with the PHB protective layer, while TEM only depicts the silver metal core (Paramelle et al.,

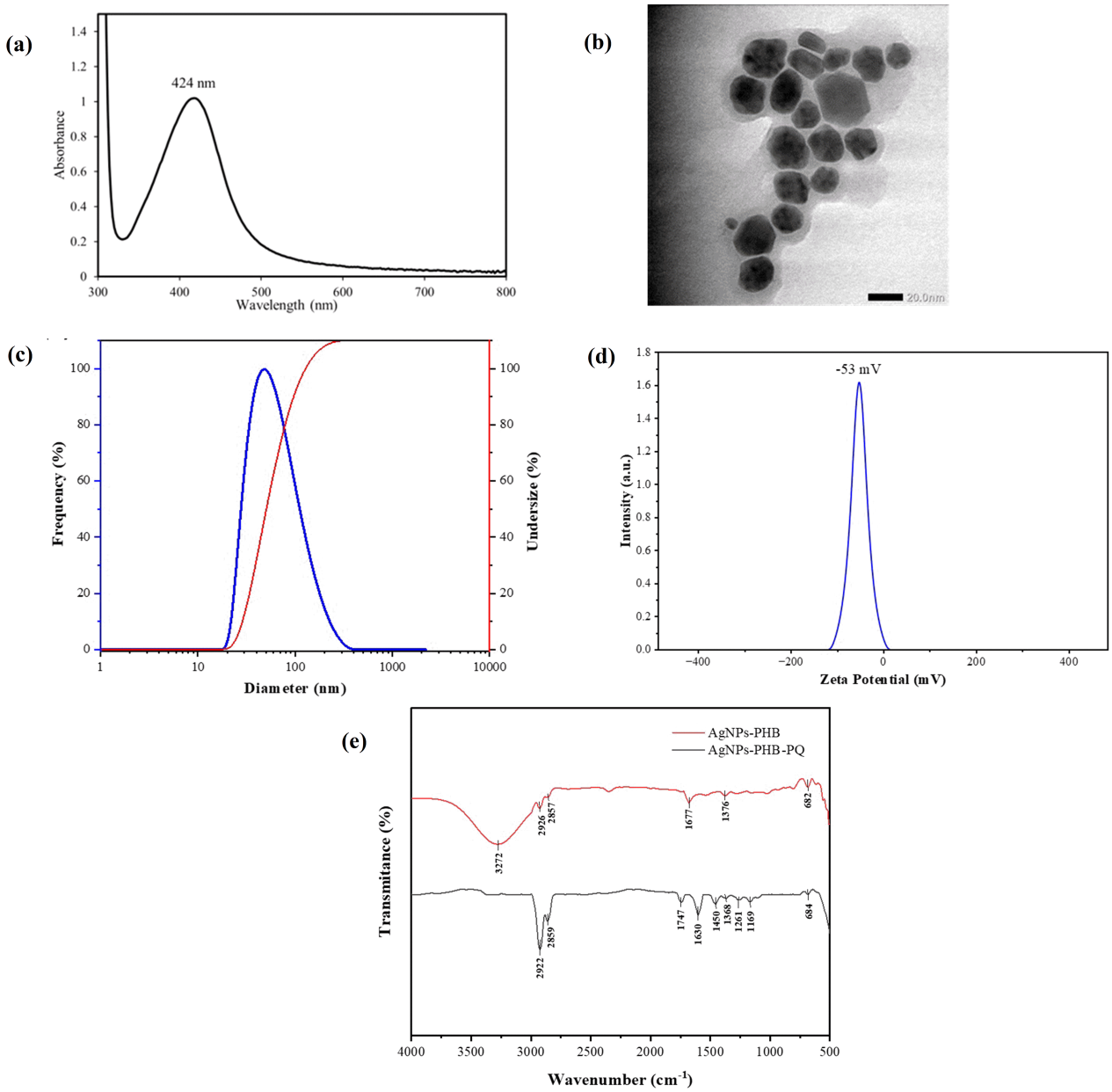

Figure 4. a) SPR Spectra of AgNPs-PHB, b) TEM Image of AgNPs-PHB, c) Distribution of AgNPs-PHB Sizes Based on PSA Analysis, d) Zeta Potential Distribution Profile of AgNPs–PHB e) ATR-IR Spectra of AgNPs-PHB and AgNPs-PHB-PQ

2014). The core size at the nanometer scale is consistent with the UV–Vis analysis results, where the SPR peak appears at 424 nm, consistent with the characteristics of silver nanoparticles smaller than 100 nm. The PDI value of 0.392 indicates a moderate size distribution, while the zeta potential value of –53 mV indicates excellent colloidal stability. The combination of these characterization results confirms that the obtained AgNPs–PHB are silver nanoparticles of nanoscale size, relatively uniform, and stable in suspension.

To ensure that the synthesized AgNPs-PHB are nano-sized, AgNPs-PHB were measured using a PSA instrument through the Dynamic Light Scattering (DLS) technique. Based on the PSA analysis results, a polydispersity index (PDI) value of 0.392 and a peak in the region around 68.5 nm were obtained (Figure 4c). According to DLS standards and guidelines, the diversity and size distribution of silver nanoparticles can be determined from the PDI value. A PDI value in the range of 0.1–0.4 indicates a moderate size distribution. Therefore, AgNPs-PHB can be considered to be in the nanometre scale and exhibit homogeneous polydispersity (Takechi-Haraya et al., 2022).

Zeta potential was used as a parameter to assess the sta-

Table 3. %RSD Values for Reproducibility (Interday Precision)

PQ (mole L^{-1})	Color Intensity						Average	%RSD
	Day I	Day II	Day III	Day IV	Day V	Day VI		
1.0×10^{-3}	0.0110	0.0113	0.0107	0.0112	0.0108	0.0113	0.0111	1.68%
6.0×10^{-3}	0.0484	0.0492	0.0476	0.0489	0.0479	0.0490	0.0485	1.81%
1.0×10^{-2}	0.0737	0.0755	0.0719	0.0747	0.0725	0.0751	0.0739	1.92%
						%RSD Average		1.80%

bility of colloidal nanoparticles in suspension. Zeta potential was measured using the Laser Doppler Electrophoresis (LDE) method. The zeta potential value obtained for AgNPs–PHB was –53 mV, which falls into the high negative category (Figure 4d). Zeta potential values above ±30 mV generally indicate the presence of strong electrostatic repulsive forces between particles, making the colloidal system stable and less prone to aggregation (Sękowski et al., 2020). The large negative value in AgNPs–PHB stems from the negative charge on the particle surface, which is likely contributed by the carboxylate functional groups of PHB. This electrostatic stability ensures that the particles remain well dispersed in the liquid medium. Additionally, the PHB coating may contribute to steric stabilization, so that even if the zeta potential decreases due to changes in the medium or environmental conditions, AgNPs–PHB remain resistant to aggregation.

ATR-IR analysis was employed to identify potential functional groups and to elucidate the formation mechanism of AgNPs–PHB. The ATR-IR spectra of AgNPs–PHB and AgNPs–PHB–PQ are presented in Figure 4e. In the spectrum of AgNPs-PHB, a broad absorption band is observed at approximately 3272 cm^{-1}, corresponding to the O–H stretching vibration of carboxylic or phenolic groups, which is broadened due to hydrogen bonding and partial deprotonation (Pasieczna-Patkowska et al., 2025). The absorption bands at 2857–2926 cm^{-1} are assigned to C–H stretching vibrations of aliphatic and aromatic groups (Zhang et al., 2025). A distinct band near 1677 cm^{-1} is attributed to the C=O stretching vibration of carboxylate groups (or conjugated C=O/C=C stretching in aromatic structures) (Pasieczna-Patkowska et al., 2025). The band observed at 1376 cm^{-1} is associated with C–O stretching vibrations of phenolic or ester groups, while the absorption at approximately 682 cm^{-1} may be related to Ag–O or metal–ligand stretching vibrations in the low-frequency region (Zhang et al., 2025).

3.2 Interaction between Paraquat (PQ) and AgNPs-PHB

The interaction between PQ and AgNPs-PHB was conducted in μPAD media. μPAD media consists of two parts, namely the detection zone and the hydrophobic part. The hydrophobic part was created to prevent the solvent from seeping out of the detection zone. Before being applied to paraquat measurements, the μPAD media, which had been printed according to

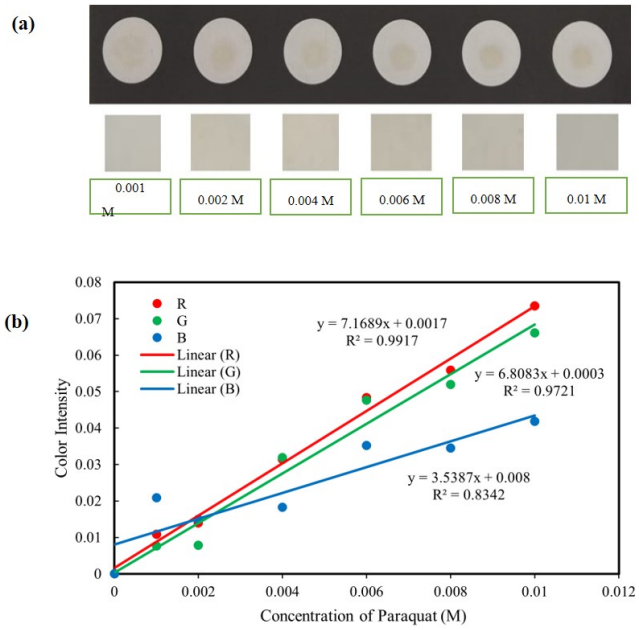

Figure 5. a) Visual Color Changes of μPAD After Reaction with Paraquat at Different Concentrations, b) Standard Curve of Paraquat

the pattern, were heated in an oven at 170 °C for 30 minutes. The purpose of heating was to allow the printer ink to be absorbed into the μPAD filter paper (Moulahoum, 2023). The ink used was a wax-based ink, which is water-resistant because the ink is hydrophobic, while water is hydrophilic.

AgNPs-PHB interacting with PQ triggers the formation of nanoparticle aggregation. This interaction is characterized by a change in the color of the AgNPs-PHB solution from yellow to grey. The mechanisms involved include electrostatic interactions and the formation of charge-transfer complexes through π–π stacking of aromatic rings (Rohit et al., 2016; Shariati and Khayatian, 2020), where PQ acts as an electron pair acceptor and the carboxylic or hydroxyl groups in AgNPs-PHB act as a donor. The interaction between PQ and the PHB layer covering the AgNPs positions PQ as a bridge connecting the nanoparticles (Gusrizal et al., 2020).

As shown in Figure 4e, the IR spectra demonstrate the interaction between PQ and AgNPs–PHB through characteris-

Table 4. Recovery Results of PQ in Different Water Samples Using the Spiking Method

Water Samples	Spiked (M)	Measured Concentration (M)	%Recoveries
Tap water	2.0×10^{-3}	2.01×10^{-3}	100.5
	4.0×10^{-3}	3.99×10^{-3}	99.75
	8.0×10^{-3}	8.12×10^{-3}	101.5
Drainage water	2.0×10^{-3}	2.05×10^{-3}	102.5
	4.0×10^{-3}	4.04×10^{-3}	101
	8.0×10^{-3}	7.98×10^{-3}	99.75
Well water	2.0×10^{-3}	1.99×10^{-3}	99.7
	4.0×10^{-3}	4.09×10^{-3}	102.25
	8.0×10^{-3}	8.16×10^{-3}	102

tic vibrational changes. The absorption bands at 2859–2922 cm^{-1} are attributable to C–H stretching vibrations of aliphatic or aromatic groups (Zhang et al., 2025). While the sharp peak at 1747 cm^{-1} is assigned to the C=O stretching of the ester or carboxyl group (Akhatova et al., 2023). The band at 1630 cm^{-1} is attributed to the C=C stretching vibration of the aromatic pyridinium ring of PQ (Akhatova et al., 2023; Pasieczna-Patkowska et al., 2025). The peaks at 1450 cm^{-1} and 1368 cm^{-1} correspond to C–H bending (scissoring) and C–N stretching vibrations, respectively (Akhatova et al., 2023). The absorption at 1261 cm^{-1} and 1169 cm^{-1} can be assigned to C–O stretching vibrations of ester and phenolic groups from PHB, respectively (Akhatova et al., 2023). Meanwhile, the low-frequency band at 684 cm^{-1} may be related to Ag–O or metal–ligand stretching vibrations in the low-frequency region (Zhang et al., 2025).

The most prominent difference between the IR spectra of AgNPs–PHB and AgNPs–PHB–PQ was the disappearance of the broad O–H stretching band around 3200 cm^{-1} in the latter. This disappearance indicated that both hydroxyl and carboxyl groups of PHB were involved in interactions with PQ molecules. These results confirmed that electrostatic interactions occurred between the negatively charged oxygen atoms (O^-) of the carboxylate and phenolic groups in PHB and the positively charged nitrogen atoms (N^+) in the pyridinium rings of PQ, leading to molecular adsorption and enhanced structural stability of the AgNPs-PHB composite. This phenomenon is analogous to the electrostatic and hydrogen-bonding interactions reported for amino-functionalized graphene oxide (GO–NH_2) with cationic dyes such as Rhodamine B and divalent metal ions (Ni^{2+}), where the negatively charged oxygen-containing groups (–COO^-, –O^-) on GO–NH_2 act as the primary sites for electrostatic attraction toward the positively charged nitrogen (N^+) of Rhodamine B, while free amine groups (–NH_2) contribute mainly through hydrogen bonding (Çelebi and Gökirmak Söğüt, 2022).

3.3 Linearity of the Paraquat (PQ) Standard Curve

The linearity of a standard curve is determined by measuring the color values (Rs, Gs, and Bs) resulting from the reaction between the AgNPs-PHB solution and the PQ standard. The test was conducted on µPAD media by immobilizing AgNPs-PHB and then reacting it with PQ at various concentrations. Color value measurements were performed on the grey detection zone using ImageJ software, where images were previously captured using a smartphone. Color value was measured during three measurements (repetitions). The color value was then converted to a logarithmic scale to obtain the color intensity according to Lambert-Beer's law (Equations 1, 2, and 3). Similar to absorbance, color intensity has a value that is directly proportional to concentration. The higher the concentration of a substance, the higher the color intensity value (Table 1).

The relationship between paraquat concentration and color intensity exhibited a clear linear trend. As illustrated in Figure 5a, the μPAD displayed a progressive and distinguishable color development with increasing paraquat concentration, indicating a concentration-dependent colorimetric response. Quantitative analysis was subsequently performed by extracting the RGB color intensity values and fitting them to linear regression models, as shown in Figure 5b. Among the three color channels, the red channel demonstrated the highest coefficient of determination (R^2 = 0.9917), reflecting superior linearity and sensitivity toward paraquat detection compared to the green and blue channels. These results confirm that the red channel provides the most reliable analytical response and was therefore selected as the primary signal for further quantitative analysis.

To determine the LOD and LOQ in this test, data on the concentration variation of PQ (1.0×10^{-3} – 1.0×10^{-2} M) and the linear regression Equation for red color intensity was y = 7.1689x + 0.0017 (R^2 = 0.9917). Based on the formula in Equations 5 and 6, the LOD and LOQ values were obtained as 0.00060 M and 0.0020 M, respectively. The LOD calculation results indicate that this analytical method is capable of detecting the presence of PQ at a minimum concentration of 0.0006 M. The LOQ indicates that the analytical method can accurately and precisely measure PQ concentrations at 0.0020 M or higher.

Although the concentration range used (1.0×10^{-3} – 1.0×10^{-2} M) exceeds typical paraquat levels detected in natural water, this concentration range was intentionally selected to

Table 5

Samples	Materials	Technique	LOD	Linear Range	%Recoveries	References
Tap, drainage, and well water	AgNPs-PHB	Colorimetry (Micro Paper Analytical Device)	0.00060 M	0.001 – 0.01 M	99.7–102.5%	Present Work
Soil	Citrate-AgNPs	Paper-based Colorimetry	10 μM	10 – 100 μM	74.2 – 95.2%	(Bhandari et al., 2024)
Tap, river, lake water, and fruit	AuNPs/caboxylate pillar[5]arenes	Electrochemical	0.73 nM	3.8 – 10 μM	92.0 – 106%	(Xiong et al., 2022)
Water and vegetables	Sodium dithionite	Colorimetry (Micro Paper Analytical Device)	20 μM	2.0×10^{-5} – 2.0×10^{-3} M	97.20 – 106.85%	(Sangsum and Saetear, 2022)
Canal water	AgNPs-PHB	Spectrophotometry UV-VIS	8.30×10^{-6} M	6.0×10^{-4} – 1.0×10^{-3} M	121%	(Gusrizal et al., 2020)
Human urine and plasma	Sodium dithionite	Spectrophotometry UV-VIS	0.74 μM	1.48 – 44.40 μM	97.3 – 101.2%	(Sha et al., 2019)
Coconut water natural water	Modified CPME with biochar	Voltammetry	7.5×10^{-9} M	3.0×10^{-8} – 1.0×10^{-6} M	95.8 – 97.5%	(Kalinke et al., 2016)
Tap, river water, wastewater	Cucurbit[7]uril & acridine orange	Spectrophotometry UV-VIS	1.61×10^{-9} M	3.0×10^{-9} – 8.0×10^{-9} M	96.7 – 101.2%	(Xing et al., 2013)

ensure a visible and measurable color change in the μPAD platform. At lower concentrations, the aggregation-induced color change becomes too subtle to be quantified accurately by RGB analysis. Nonetheless, the current study provides a critical foundation for the design optimization of μPADs for pesticide monitoring and demonstrates the feasibility of using AgNPs–PHB as an effective colorimetric sensing element for paraquat detection.

3.4 Precision

The repeatability of the μPAD method in determining PQ was performed using 6 μPADs and PQ standards with concentrations of 1.0×10^{-3}, 6.0×10^{-3}, and 1.0×10^{-2} M. The repeatability calculation results (Equation 7) are shown in Table 2, where this method provides good intraday precision with %RSD values of 1.08%, 1.79%, and 1.96% respectively for the determination of PQ at concentrations of 1.0×10^{-3}, 6.0×10^{-3}, and 1.0×10^{-2} M. So that the average intraday %RSD was 1.61%. The reproducibility shown in Table 3 also provides %RSD values of 1.68%, 1.81%, and 1.92% for the determination of PQ at 1.0×10^{-3}, 6.0×10^{-3}, and 1.0×10^{-2} M, respectively, resulting in an average interday %RSD of 1.80%.

The precision test of the μPAD method for determining PQ showed that the %RSD values obtained were good in both intraday and interday measurements. The consistent average %RSD value of less than 2% in both tests confirms that the μPAD method has excellent precision, is capable of providing stable results, and can be reproduced under different measurement conditions (Moulahoum, 2023).

3.5 Determination of PQ in Water Samples

The validated μPAD device was then used to analyze paraquat (PQ) in various water samples. Tests were conducted on tap water, drainage water, and well water using the spiking method, which involves adding PQ standard solutions at concentrations of 2.0×10^{-3}, 4.0×10^{-3}, dan 8.0×10^{-3} M. This approach aims to evaluate measurement accuracy based on Equation (4). The results in Table 4 show that the PQ recovery percentage ranged from 99.7% to 102.5%. These findings suggest that the spiking method employed can achieve high detection accuracy for PQ in various types of water samples (Sangsum and Saetear, 2022). Therefore, this procedure is reliable for water quality analysis, particularly for monitoring pesticide contaminants such as PQ. For comparison, several methods have been reported for determining PQ levels in various samples, as shown in Table 5.

The recoveries reported for PQ determination methods vary widely, ranging from 74.2% to 121%. This variation reflects differences in accuracy influenced by the analytical technique, sample matrix, and materials applied. The recoveries obtained in this study (99.7–102.5%) fall within the ideal range recommended for analytical method validation (98–102%), indicating excellent accuracy and comparable performance to UV-Vis spectrophotometric methods. Therefore, the developed μPAD can be considered a reliable tool for accurate PQ analysis in water samples (Xiong et al., 2022). The method demonstrates excellent accuracy and reproducibility when applied to spiked water matrices, including tap, drainage, and well water. These results suggest that the μPAD can be effectively employed for rapid on-site screening of paraquat contamination in areas where elevated pesticide levels are suspected, such as agricultural runoff, wastewater near herbicide application zones, or industrial effluents.

Although the developed μPAD demonstrated good analytical performance, the obtained limit of detection (LOD) value of 0.00060 M is relatively high compared to the paraquat concentration levels typically found in real environmental waters, which are generally in the range of 10^{-9}–10^{-6} M. This relatively high LOD indicates that the present device is less sensitive for trace-level detection of paraquat in natural waters. The limitation may be attributed to the intrinsic colorimetric principle of μPADs, which relies on visible nanoparticle aggregation rather than on more sensitive electrochemical or

fluorescence-based amplification mechanisms. Nevertheless, the proposed μPAD offers several important advantages: it is simple, low-cost, portable, and environmentally friendly, as it eliminates the use of organic solvents and minimizes chemical waste generation in accordance with the principles of green analytical chemistry. These features make it highly practical for rapid on-site screening and laboratory-scale monitoring of paraquat contamination, particularly in areas with high pollution risk or during emergency response situations.

4. CONCLUSIONS

A colorimetric μPAD based on silver nanoparticles stabilized with *p*-hydroxybenzoate (AgNPs–PHB) was successfully developed for the determination of paraquat (PQ). The μPAD demonstrated good analytical performance with linear response in the concentration range of 1.0×10^{-3} – 1.0×10^{-2} M, LOD of 6.0×10^{-4} M, and recovery values of 99.7–102.5% for spiked water samples. The analytical response was attributed to the aggregation of AgNPs–PHB induced by paraquat, producing a measurable color shift suitable for RGB-based quantification. Although the detection limit remains higher than environmental paraquat levels, the system offers promising potential for rapid, low-cost on-site screening. Further optimization such as integrating preconcentration zones or smartphone-assisted image processing may enhance its sensitivity for real environmental monitoring applications.

5. ACKNOWLEDGEMENT

The authors gratefully acknowledge the financial support from the Faculty of Mathematics and Natural Sciences, Universitas Tanjungpura, through the DIPA funding scheme under contract number 2782/UN22.8/PT.01.05/2024.

REFERENCES

Akhatova, F., S. Konnova, M. Kryuchkova, S. Batasheva, K. Mazurova, A. Vikulina, D. Volodkin, and E. Rozhina (2023). Comparative Characterization of Iron and Silver Nanoparticles: Extract-Stabilized and Classical Synthesis Methods. *International Journal of Molecular Sciences*, **24**(11); 9274

Anushka, A. Bandopadhyay, and P. K. Das (2022). Paper Based Microfluidic Devices: A Review of Fabrication Techniques and Applications. *The European Physical Journal Special Topics*, **232**(6); 781–815

Beshana, S., A. Hussen, S. Leta, and T. Kaneta (2022). Microfluidic Paper Based Analytical Devices for the Detection of Carbamate Pesticides. *Bulletin of Environmental Contamination and Toxicology*, **109**(2); 344–351

Bhandari, S., V. S. Parihar, M. Kellomäki, and M. Mahato (2024). Highly Selective and Flexible Silver Nanoparticles-Based Paper Sensor for On-Site Colorimetric Detection of Paraquat Pesticide. *RSC Advances*, **14**(39); 28844–28853

Çelebi, M. and E. Gökirmak Söğüt (2022). High-Efficiency Removal of Cationic Dye and Heavy Metal Ions from Aqueous Solution Using Amino-Functionalized Graphene Oxide, Adsorption Isotherms, Kinetics Studies, and Mechanism. *Turkish Journal of Chemistry*, **46**(5); 1577–1593

Chandra, A., K. A. Shah, S. Mahato, M. S. Bhattacharjee, and T. Mandal (2021). Paraquat Poisoning. *BMJ Case Reports*, **14**(11); e246585

Firdaus, M. L., A. Aprian, N. Meileza, M. Hitsmi, R. Elvia, L. Rahmidar, and R. Khaydarov (2019). Smartphone Coupled with a Paper-Based Colorimetric Device for Sensitive and Portable Mercury Ion Sensing. *Chemosensors*, **7**(2); 25

Franco, D. S. P., J. Georgin, E. C. Lima, and L. F. O. Silva (2022). Advances Made in Removing Paraquat Herbicide by Adsorption Technology: A Review. *Journal of Water Process Engineering*, **49**; 102988

Goulet, P. J. G. and R. F. Aroca (2004). Chemical Adsorption of Salicylate on Silver: A Systematic Approach to the Interpretation of Surface-Enhanced Vibrational Spectra. *Canadian Journal of Chemistry*, **82**(6); 987–997

Gusrizal (2017). Sintesis Nanopartikel Perak Melalui Reduksi Ion Perak dengan Asam 2-, 3-, dan 4-Hidroksibenzoat serta Aplikasinya untuk Penentuan Parakuat

Gusrizal, S. J. Santosa, E. S. Kunarti, and B. Rusdiarso (2016). Dual Function of p-Hydroxybenzoic Acid as Reducing and Capping Agent in Rapid and Simple Formation of Stable Silver Nanoparticles. *International Journal of ChemTech Research*, **9**(9); 472–482

Gusrizal, S. J. Santosa, E. S. Kunarti, and B. Rusdiarso (2018). Two Highly Stable Silver Nanoparticles: Surface Plasmon Resonance Spectra Study of Silver Nanoparticles Capped with m-Hydroxybenzoic Acid and p-Hydroxybenzoic Acid. *Molekul*, **13**(1); 30–37

Gusrizal, S. J. Santosa, E. S. Kunarti, and B. Rusdiarso (2020). Silver Nanoparticles Capped with p-Hydroxybenzoic Acid as a Colorimetric Sensor for the Determination of Paraquat. *Indonesian Journal of Chemistry*, **20**(3); 688–696

Heydebreck, F. (2021). Monitoring of Paraquat in Soya Products Intended for Animal Feed. *International Journal of Food Contamination*, **8**(1); 9

Kalinke, C., A. S. Mangrich, L. H. Marcolino-Junior, and M. F. Bergamini (2016). Carbon Paste Electrode Modified with Biochar for Sensitive Electrochemical Determination of Paraquat. *Electroanalysis*, **28**(4); 764–769

Khatoon, R., M. K. Rai, and J. K. Rai (2013). Low Cost Spectrophotometric Determination of Paraquat in Environmental and Biological Samples. *Recent Research in Science and Technology*, **5**(2); 4–6

Kumar Majumder, K., J. B. Sharma, M. Kumar, S. Bhatt, and V. Saini (2020). A Review on Paraquat Poisoning. *Pharmacophore*, **11**(1); 115–121

Lima, T. L., M. A. Nicoletti, C. Munhoz, G. R. de Abreu, J. Z. Magalhães, E. L. R. Ricci, P. A. F. Waziry, J. N. A. da Costa, A. C. N. Antônio, and A. R. Fukushima (2018). Determination of Paraquat in Several Commercially Available Types of Rice. *Food and Nutrition Sciences*, **9**(12); 1368–1376

Madaniyah, L., S. Fiddaroini, E. K. Hayati, M. F. Rahman, and

A. Sabarudin (2025). Stability of Biologically Synthesized Silver Nanoparticles (AgNPs) Using *Acalypha indica* L. Plant Extract as Bioreductor and Their Potential as Anticancer Agents Against T47D Cells. *Science and Technology Indonesia*, **10**(1); 101–110

Moulahoum, H. (2023). Dual Chromatic Laser-Printed Microfluidic Paper-Based Analytical Device (μPAD) for the Detection of Atrazine in Water. *ACS Omega*, **8**(44); 41194–41203

Pan, S., L. Wang, Q. Qiu, and Q. He (2022). Determination of Paraquat and Diquat Residues in Urine Samples Based on Solid-Phase Extraction and Ultra Performance Liquid Chromatography–High Resolution Mass Spectrometry. *Chinese Journal of Chromatography*, **40**(12); 1087–1094

Paramelle, D., A. Sadovoy, S. Gorelik, P. Free, J. Hobley, and D. G. Fernig (2014). A Rapid Method to Estimate the Concentration of Citrate Capped Silver Nanoparticles from UV–Visible Light Spectra. *Analyst*, **139**(19); 4855–4861

Pasieczna-Patkowska, S., M. Cichy, and J. Flieger (2025). Application of Fourier Transform Infrared (FTIR) Spectroscopy in Characterization of Green Synthesized Nanoparticles. *Molecules*, **30**(3); 684

Pizzutti, I. R., G. M. E. Vela, A. de Kok, J. M. Scholten, J. V. Dias, C. D. Cardoso, G. Concenço, and R. Vivian (2016). Determination of Paraquat and Diquat: LC–MS Method Optimization and Validation. *Food Chemistry*, **209**; 248–255

Rahman, A. K. M. F., S. Al Kafi, and Z. Naiem (2024). Study on Clinical Profile and Treatment Outcome of Acute Paraquat Poisoning in an Intensive Care Unit in Bangladesh. *Journal of Medicine*, **25**(2); 129–135

Rohit, J. V., H. Basu, R. K. Singhal, and S. K. Kailasa (2016). Development of p-Nitroaniline Dithiocarbamate Capped Gold Nanoparticles-Based Microvolume UV–Vis Spectrometric Method for Facile and Selective Detection of Quinalphos Insecticide in Environmental Samples. *Sensors and Actuators B: Chemical*, **237**; 826–835

Sangsum, C. and P. Saetear (2022). All-Step-in-One Test Kit for Paraquat Detection in Water and Vegetable Samples. *Analytica*, **3**(1); 92–105

Sękowski, S., E. Olchowik-Grabarek, W. Więckowska, A. Veiko, L. Oldak, E. Gorodkiewicz, E. Karamov, N. Abdulladjanova, S. Mavlyanov, E. Lapshina, I. B. Zavodnik, and M. Zamaraeva (2020). Spectroscopic, Zeta-Potential and Surface Plasmon Resonance Analysis of Interaction between Potential Anti-HIV Tannins with Different Flexibility and Human Serum Albumin. *Colloids and Surfaces B: Biointerfaces*, **194**; 111175

Sha, O., B. Cui, H. Liu, Y. Wang, X. Chen, L. Chen, and S. Wang (2019). A Simple and Rapid Method for Determination of Paraquat in Human Urine and Plasma by Improved Solid Adsorption Using Equipment Built In-House. *Journal of the Iranian Chemical Society*, **16**(10); 2071–2080

Shariati, S. and G. Khayatian (2020). Microfluidic Paper-Based Analytical Device Using Gold Nanoparticles Modified with N,N′-Bis(2-Hydroxyethyl)dithiooxamide for Detection of Hg(II) in Air, Fish and Water Samples. *New Journal of Chemistry*, **44**(43); 18662–18667

Stuart, A. M., C. N. Merfield, F. G. Horgan, S. Willis, M. A. Watts, F. Ramírez-Muñoz, J. S. U, L. Utyasheva, M. Eddleston, M. L. Davis, L. Neumeister, M. R. Sanou, and S. Williamson (2023). Agriculture without Paraquat Is Feasible without Loss of Productivity–Lessons Learned from Phasing Out a Highly Hazardous Herbicide. *Environmental Science and Pollution Research*, **30**(7); 16984–17008

Sununta, S., P. Rattanarat, O. Chailapakul, and N. Praphairaksit (2018). Microfluidic Paper-Based Analytical Devices for Determination of Creatinine in Urine Samples. *Analytical Sciences*, **34**(1); 109–113

Takechi-Haraya, Y., T. Ohgita, Y. Demizu, H. Saito, K.-i. Izutsu, and K. Sakai-Kato (2022). Current Status and Challenges of Analytical Methods for Evaluation of Size and Surface Modification of Nanoparticle-Based Drug Formulations. *AAPS PharmSciTech*, **23**(5); 150

Takino, M., S. Daishima, and K. Yamaguchi (2000). Determination of Diquat and Paraquat in Water by Liquid Chromatography/Electrospray–Mass Spectrometry Using Volatile Ion-Pairing Reagents. *Analytical Sciences*, **16**(7); 707–711

Wang, Y., Y.-S. Li, Z. Zhang, and D. An (2003). Surface-Enhanced Raman Scattering of Some Water-Insoluble Drugs in Silver Hydrosols. *Spectrochimica Acta Part A: Molecular and Biomolecular Spectroscopy*, **59**(3); 589–594

Xing, X., Y. Zhou, J. Sun, D. Tang, T. Li, and K. Wu (2013). Determination of Paraquat by Cucurbit[7]uril Sensitized Fluorescence Quenching Method. *Analytical Letters*, **46**(4); 694–705

Xiong, Y., T. Ma, H. Zhang, L. Qiu, S. Chang, Y. Yang, and F. Liang (2022). Gold Nanoparticle Functionalized Nanopipette Sensors for Electrochemical Paraquat Detection. *Microchimica Acta*, **189**(7); 234

Yar, A., T. M. Ansari, A. Raza, and S. Manzoor (2022). Development and Validation of HPLC–UV Method for Determination of Paraquat in Raw and Commercial Samples. *Pakistan Journal of Analytical & Environmental Chemistry*, **23**(1); 148–155

Zhang, J., Y. Chen, Y. Xu, Z. Zhao, and X. Xu (2025). Salicylic Acid-Mediated Silver Nanoparticle Green Synthesis: Characterization, Enhanced Antimicrobial, and Antibiofilm Efficacy. *Pharmaceutics*, **17**(4); 532

Zhao, M., Q. Wang, M. Shi, Z. Sun, H. Tang, and X. Ge (2023). Determination of Paraquat in Arabidopsis Tissues and Protoplasts by UHPLC–MS/MS. *International Journal of Molecular Sciences*, **24**(13); e4642